JMEPEG (2020) 29:2658–2666
https://doi.org/10.1007/s11665-020-04762-5

©ASM International
1059-9495/$19.00

Temperature-Dependent Isothermal Oxidation Behavior of a Ni-20Cr-18W Superalloy in Static Air

Jiaqi Shi, Tiebang Zhang, Bing Wang, Xuhu Zhang, Lin Song, and Rui Hu

(Submitted April 1, 2019; in revised form March 14, 2020; published online April 10, 2020)

The oxidation behavior of superalloys has attracted more attention due to the increasing service temperature of components in aero-engines. In this study, the isothermal oxidation behavior of a Ni-20Cr-18W superalloy has been investigated at 900 and 1000 °C in air. The oxidation kinetics follows a parabolic oxidation law at both temperatures. The outer layer of the oxide scales is mainly composed of mixed oxides of Cr_2O_3 and $NiCr_2O_4$, and the inner layer is Cr_2O_3 at 900 °C. During oxidizing at 1000 °C, the oxide scales evolve from dense Cr_2O_3 single-layer structure to double-layer structure which consists of inner Cr_2O_3 layer and outer layer composed of lots of $NiCr_2O_4$, Cr_2O_3 and a small amount of NiO, and the size and content of $NiCr_2O_4$ are relatively larger than that of 900 °C. The internal oxidation zone dispersed with Al_2O_3 is formed under the oxide scales at both 900 and 1000 °C. The obvious cracks are observed at the interface between the outer layer and the inner layer, which is ascribed to the generation of growth stress and thermal stress. Compared with the oxidation behavior at 900 °C, the cracking and spalling in oxide scales are much severer at 1000 °C due to the greater internal stress. The experimental Ni-20Cr-18W superalloy is oxidized through the inward diffusion of oxygen and the outward diffusion of metal elements.

Keywords isothermal oxidation, Ni-20Cr-18W superalloy, oxidation mechanism, oxide scales

1. Introduction

Ni-based superalloys are widely used in aero-engine turbine blades, turbine disks, oil and electricity industries due to their excellent mechanical strength, oxidation resistance and corrosion resistance at high temperature (Ref 1, 2). However, when Ni-based superalloys are exposed to harsh service conditions, high-temperature oxidation is a key factor for the failure of components. During oxidation process, the integrity of alloy surface is deteriorated, and Al, Cr and Ni elements on the surface are depleted, which can lead to the loss of surface strength, the initiation of cracks and premature failure of the alloy (Ref 3-5). Meanwhile, the integrity of the oxide scales is destroyed by cracking and spalling, which accelerate the further oxidation of alloys. Alloying and protective coatings are usually used to improve the oxidation resistance of superalloys (Ref 6-9). However, for assessing the integrity of the oxide scales on alloy as well as beneficial effects of alloying or coatings, it is necessary to study the oxidation behavior of bare superalloys.

In order to improve the mechanical properties of superalloys, the solid solution strengthening elements such as Co, Cr, W, Re and Mo are often added, and precipitation strengthening elements such as Al, Ti and Ta are also added to form γ′-Ni_3(Al,Ti,Ta) in γ-matrix (Ref 1, 10). In particular, Al, Cr and Si elements not only play a strengthening role, but provide superior oxidation resistance at elevated temperatures (Ref 6, 11, 12). Combined with precipitation strengthening, the solid solution strengthening is used to strengthen the Ni-20Cr-18W superalloy. The addition of a large amount of solid solution strengthening element Cr enhances mechanical properties of Ni-Cr-W-based superalloys, and also improves the oxidation resistance of the alloys. The oxidation resistance of superalloys depends on the formation of continuous, stable and dense oxide scales on the alloy surface. The oxide scale composed of Al_2O_3 or Cr_2O_3 has been proven to prevent the inward diffusion of oxygen and the outward diffusion of alloy elements, which significantly decrease the oxidation rate and improve the oxidation resistance of superalloys (Ref 13-16).

The oxidation resistance of Ni-based superalloys is affected by these factors, including type and content of alloying elements and subsequent surface treatment processes. During the past decades, numerous scholars have performed a lot of work on the oxidation behavior of Ni-based superalloys. The addition of Al and Si elements can significantly improve the oxidation resistance of alloy by inhibiting the formation of transient oxides. Mn is detrimental to the oxidation resistance by facilitating the formation of NiO, $NiCr_2O_4$ and $NiWO_4$ (Ref 6). Wang et al. (Ref 17) have revealed that the addition of La can obviously improve the bonding ability between the substrate and the oxide scale, thus improving the oxidation resistance of Ni-20Cr-18W-1Mo alloy at 1100 °C. Yun et al. (Ref 18) have observed that the porosity of oxide scales increases with sulfur content. The high porosity results in an increase in spallation, which accelerates depletion of Cr and Al elements. Wu et al. (Ref 19) have reported that sand blasting pre-treatment cannot change significantly oxidation kinetics of K38G superalloy, but can refine the crystalline size and change the growing mode of oxide scales by changing the diffusion of Cr, which subsequently results in the variation of surface morphologies of oxide scales. The oxidation kinetics of IN-

Jiaqi Shi, Tiebang Zhang, Lin Song, and **Rui Hu**, State Key Laboratory of Solidification Processing, Northwestern Polytechnical University, Xi'an 710072, China; and **Bing Wang** and **Xuhu Zhang**, Spaceflight Material and Technology Research Institute, Beijing 100076, China. Contact e-mail: tiebangzhang@nwpu.edu.cn.

738LC alloy follows a parabolic rate law at 950 °C. The oxide scales can be divided into three layers, the outer and mid layers enriched by TiO_2 and Cr_2O_3, $NiCr_2O_4$ oxides, respectively, and the innermost layer consists of discontinuous Al_2O_3 and matrix alloy (Ref 20). Although the addition of alloying elements and the surface treatment of alloys can improve the oxidation resistance of alloys, their effects are limited and may result in the deterioration of the mechanical properties of alloys. Further study on the oxidation behavior of superalloy substrate is necessary for the subsequent development of alloys with excellent oxidation resistance. At present, substantial studies on Ni-Cr-W-based superalloys oxidation mainly concentrate on phase composition and oxidation kinetics, but there are a few studies on the cracking of oxide scales and oxidation mechanism.

The oxidation resistance of Ni-Cr-W-based superalloys mainly depends on the formation of Cr_2O_3 oxide scale. However, Cr_2O_3 reacts with oxygen at 1000 °C or above (Ref 5, 21), so it is necessary to study the effects of critical temperature (1000 °C) on the oxidation behavior of alloys. Moreover, 900-1000 °C is a typical material surface temperature of gas turbine engines. In this study, the oxidation behavior of a Ni-20Cr-18W superalloy is studied at both 900 and 1000 °C in static air. The oxidation kinetics of the Ni-20Cr-18W superalloy at different temperatures is investigated. The oxidation behavior of alloy and the microstructure of oxide scale are discussed. Meanwhile, oxidation mechanism of the Ni-20Cr-18W superalloy and the causes of cracking and spalling in oxide scales during oxidation are analyzed in detail. In particular, the study of the formation, evolution and cracking of the oxide scale as well as the discussion of the oxidation mechanism can provide more theoretical basis for the subsequent increase in oxidation resistance and service temperature of Ni-Cr-W-based superalloys through the addition of alloying elements.

2. Experimental Procedures

2.1 Materials

The chemical composition (wt.%) of the rolled-state Ni-based superalloy used in this work is shown in Table 1. The addition of Cr, W and Mo elements can play a solid solution strengthening role, and the addition of a large amount of Cr element can also improve the oxidation resistance of the alloy. The alloy was first prepared by vacuum induction melting (VIM), and then the alloy was re-melted twice by vacuum arc re-melting (VAR). The alloy ingot was homogenized at 1200 °C for 24 h under vacuum condition. Finally, the ingot was hot-rolled into a sheet with 3 mm in thickness at 1150 °C.

Table 1 Chemical composition of Ni-20Cr-18W superalloy (wt.%) (Ref 22)

Ni	Cr	W	Mo	Al	C	La	B
Bal.	19.820	18.480	1.240	0.460	0.110	0.026	0.0028

2.2 High-Temperature Oxidation

Specimens with the dimensions of 20 mm × 10 mm × 2 mm were cut from Ni-20Cr-18W alloy plate by wire electrical discharge machine. All samples were ground to 2000 grade with SiC paper, and ultrasonically cleaned in alcohol and acetone. The isothermal oxidation test was conducted in the atmospheric environment at 900 and 1000 °C for 5, 10, 20, 40, 60, 80 and 100 h to evaluate the oxidation resistance performance of the Ni-20Cr-18W superalloy, and air can have free access to all the surfaces of the samples. Each specimen was put into an alumina crucible, and then placed in a muffle furnace. The alumina crucibles were heated for 3 h before use in order to eliminate the effect of moisture. The mass gains were measured by an electronic balance with the precision of 10^{-5} g after specimens were cooled to room temperature in air.

2.3 Characterization of Oxides

The oxidation behavior of the Ni-20Cr-18W superalloy was characterized after the oxidation experiment. The phase composition of the oxide scales was identified by x-ray diffraction (XRD-7000) using Cu Kα radiation with 2θ, 20°-90°. The surface microstructure and cross-sectional microstructure of the oxide scales after oxidation were analyzed by scanning electron microscopy (SEM) equipped with an energy-dispersive x-ray spectrometer (EDS). The element distribution of the oxide scales on the cross section of oxidized samples was analyzed by the electron probe micro-analyzer (EPMA).

3. Results and Discussion

3.1 Isothermal Oxidation Kinetics

The isothermal oxidation kinetics curves of Ni-20Cr-18W superalloy at 900 and 1000 °C in air up to 100 h are presented Fig. 1(a). It can be observed that the mass gain per unit area of the Ni-20Cr-18W superalloy increases with oxidation time at 900 and 1000 °C, and the oxidation rate at 1000 °C is higher than that at 900 °C. The total mass gain of Ni-20Cr-18W superalloy is 3.838×10^{-4} and 10.050×10^{-4} g cm^{-2} after oxidation at 900 and 1000 °C for 100 h, respectively. The mass gain at 1000 °C is about three times of that at 900 °C, which indicates that temperature has an important effect on the oxidation behavior of Ni-20Cr-18W superalloy. According to the oxidation rate at 900 and 1000 °C, the oxidation process can be divided into two stages. In the first stage of 0-20 h, the mass gain increases rapidly due to the relatively large surface area of samples that are exposed to the oxidizing environment. In addition, Cr_2O_3 has lower formation free energy than NiO (Ref 23). Therefore, it can be considered that the early oxidation stage of Ni-20Cr-18W alloy is mainly the rapid formation and growth of Cr_2O_3 oxides accompanied by fast increasing in mass. With increase in oxidation time from 20 to 100 h, the mass gain increases slowly because dense and continuous oxide scales on the alloy surface can prevent the diffusion of oxygen and alloy elements. Comparing with the mass gain per unit area of the Rene95 and EP741NP Ni-based superalloy at 900 and 1000 °C, Ni-20Cr-18W superalloy shows a better oxidation resistance (Ref 5, 23).

In order to calculate the oxidation rate constants of the Ni-20Cr-18W superalloy at 900 and 1000 °C, the mass gain of the

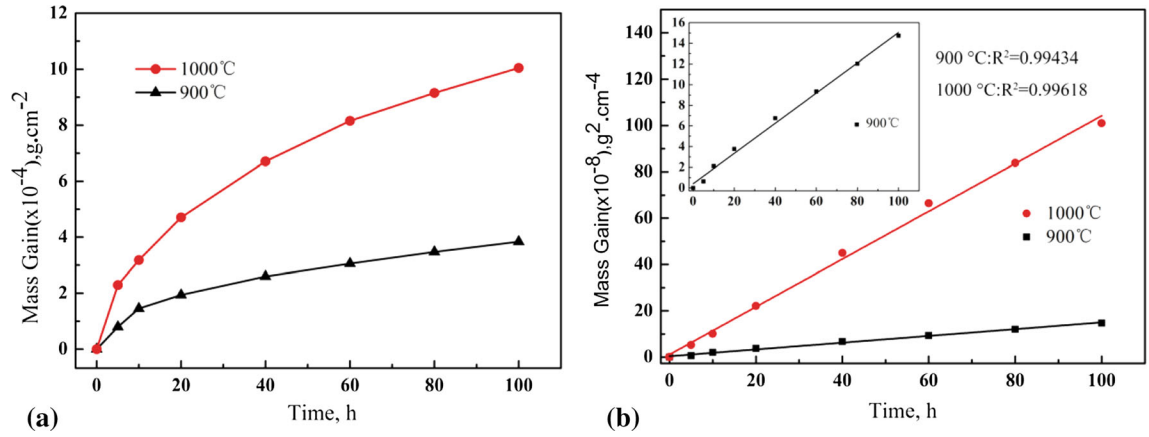

Fig. 1 (a) Oxidation kinetics curves of Ni-20Cr-18W superalloy at 900 and 1000 °C for 100 h and (b) square mass gains as a function of oxidation time

superalloy during oxidation follows a relationship of the form (Ref 23):

$$(\Delta W)^n = Kt \qquad \text{(Eq 1)}$$

where ΔW is the mass gain per unit area, n is the oxidation exponent, K is the oxidation rate constant and t is the oxidation time. Linear, logarithmic, cubic and parabolic rate laws are four oxidation kinetics models, which are used to characterize the oxidation rate (Ref 20). In order to determine the oxidation kinetics model of the Ni-20Cr-18W superalloy, the points in Fig. 1(a) are fitted by Eq. (1), and the oxidation exponent n is obtained to be 2.208 and 2.059 at 900 and 1000 °C, respectively. Compared with the four oxidation laws mentioned above, the values of n are both close to 2 at 900 and 1000 °C. Therefore, the oxidation kinetics of Ni-20Cr-18W alloy follows a parabolic oxidation law, indicating that the oxidation process is controlled by the diffusion of elements. Besides, Zheng et al. (Ref 23) and D. Saber et al. (Ref 24) have found that EP741NP and Inconel 617 alloys also follow the parabolic oxidation law, respectively. In order to be able to compare the magnitude of the oxidation rate constant K at 900 and 1000 °C, n is taken as 2. The square mass gains as a function of time at 900 and 1000 °C are plotted in Fig. 1(b). According to the linear fitting of the relationship between the square mass gains and the time, the oxidation rate constant K obtained is 4.066×10^{-13} and 2.863×10^{-12} g^2 cm^{-4} s^{-1} at 900 and 1000 °C, respectively.

3.2 Phase Constitutes and Surface Morphologies

The phase constitutes of the oxide scales on Ni-20Cr-18W alloy surface after oxidation at 900 and 1000 °C for 100 h are shown in Fig. 2, and the XRD patterns are directly from the free surface of the oxidized samples. The results show that the oxide scales on the alloy surface consist of Cr_2O_3, spinel $NiCr_2O_4$ and a small amount of NiO at 900 and 1000 °C. With the increase in temperature, the $NiCr_2O_4$ peak at 1000 °C is relatively stronger than that at 900 °C. In addition, the intensity of the matrix diffraction peak at 900 °C is obviously higher than that at 1000 °C. Although Al element has a high affinity with oxygen (Ref 25), Al_2O_3 is not observed in the oxide scales. This is mainly ascribed to the fact that the content of Al element is very low in the alloy. Also, two reasons can explain that a little of NiO is observed in the oxide scales. Firstly, Ni element has lower affinity with oxygen than Cr element, so the

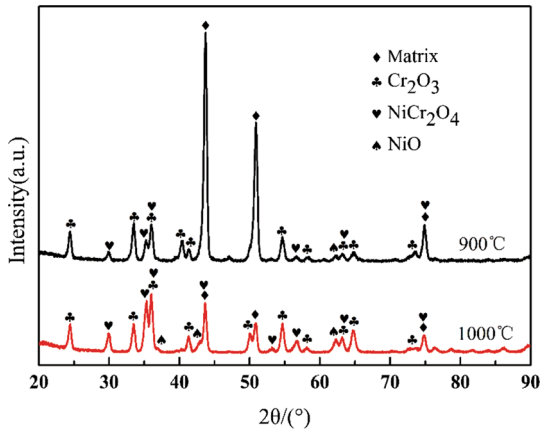

Fig. 2 XRD patterns of the oxide scales after oxidation at 900 and 1000 °C for 100 h

content of NiO is relatively less. Secondly, a large amount of NiO is consumed due to the formation of spinel $NiCr_2O_4$ (Ref 26). The oxides of W are not detected because the diffusion of W element is slow in Ni, and WO_3 oxides volatilize easily (Ref 27).

Surface morphologies of the Ni-20Cr-18W superalloy after oxidation at 900 and 1000 °C for 100 h are displayed in Fig. 3. The size and number of oxides on the alloy surface increase with temperature increasing. The oxide scales of the surface are dense after oxidation at 900 °C for 100 h in Fig. 3(a). There are two types of oxides, compact protuberance-like oxide as marked in area A, bright and loose floc-like oxide as marked in area B. Compact protuberance-like oxide consists of fine grains, while bright and loose floc-like oxide consists of relatively larger grains in Fig. 3(b). Some particles with spinel structure are distributed over loose floc-like oxide (red circle), and there are also some particles with spinel structure under the compact protuberance-like oxide (red rectangle). The results of EDS (Table 2) show that the compact protuberance-like oxide and loose floc-like oxide both consist of Cr, Ni and O elements. Although EDS results are susceptible to the flatness of sample surface and it has an inaccuracy analysis for low-Z elements, it can effectively reflect the element composition of the product. The areas A and B have different morphologies which attribute to the different nucleation and growth stages of the oxides. EDS

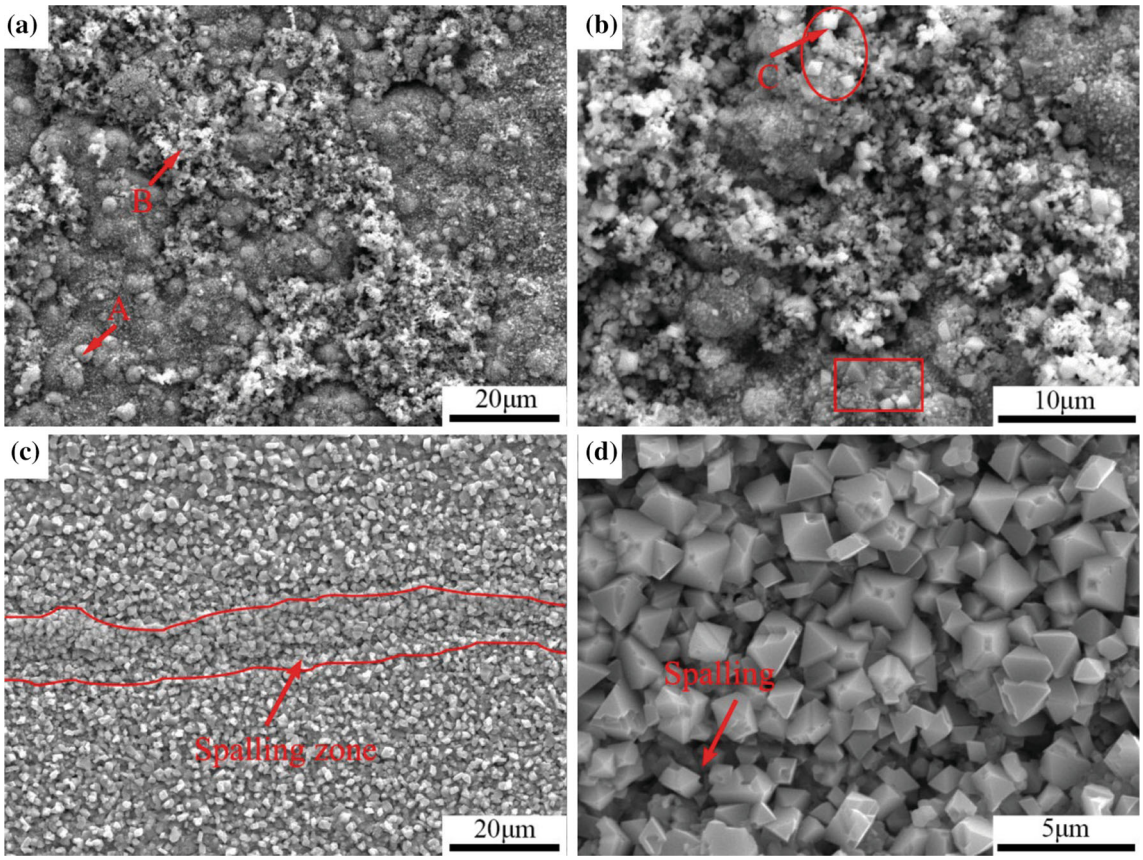

Fig. 3 The surface morphologies of the Ni-20Cr-18W superalloy after 100 h oxidation at (a) 900 °C, (b) magnification of (a), (c) 1000 °C and (d) magnification of (c)

Table 2 EDS analysis of the regions in Fig. 3 (wt.%)

Region	O	Cr	Ni
A	43.1	50.0	6.9
B	37.4	56.0	6.6
C	45.4	47.2	7.4

and XRD results indicate that the particles with spinel structure (point C) are $NiCr_2O_4$. As shown in Fig. 3(c), the surface is completely covered by uniformly distributed oxides after oxidation at 1000 °C for 100 h, and there is an obvious spalling in the central region of the surface. The oxide particles with a size of about 1- 2 μm exhibit semi-octahedral and spinel structure in Fig. 3(d). XRD results (Fig. 2) show that spinel $NiCr_2O_4$ is the dominant phase of the oxide scales after oxidation at 1000 °C. The formation of $NiCr_2O_4$ follows a reaction of $Cr_2O_3 + NiO \rightarrow NiCr_2O_4$ (Ref 28). A large amount of spinel $NiCr_2O_4$ indicates the NiO and Cr_2O_3 are not stable at high temperature. Compared with oxidation at 900 °C, severe oxidation and spalling are observed at 1000 °C.

3.3 Cross-Sectional Morphologies

Cross-sectional morphologies of the Ni-20Cr-18W superalloy after oxidation at 900 and 1000 °C for 100 h are presented in Fig. 4. It can be seen that the oxide scales are divided into two layers at both 900 and 1000 °C, and the increasing of oxidation temperature results in the formation of a thicker oxide layer. In Fig. 4(a), the thickness of the oxide layer is about 3.4 μm. The outer layer is loose, while the inner layer is dense and continuous. The chemical composition of the outer layer (point D) is (wt.%) 18.3 O, 71.9 Cr, 9.8 Ni, which corresponds to the phase composition shown in the XRD analysis. The continuous and dense inner layer consists of Cr_2O_3. In addition, it can be seen that there is an obvious internal oxidation zone under the oxide scales and some black oxides are dispersed in this area. As shown in Fig. 4(b), a thicker oxide layer is formed on the alloy surface, with a thickness of about 11.6 μm. The cross-sectional morphology at 1000 °C is similar to that at 900 °C. The outer layer has severe spalling and cracking, but the inner layer is very dense and continuous. According to the analyses of surface morphologies and the XRD, the loose outer layer contains a large amount of spinel $NiCr_2O_4$. Figure 4(c) shows the image of the internal oxidation zone after oxidation at 1000 °C for 100 h. A large number of black oxides are formed in Fig. 4(c), and the EDS results of point E are (wt.%) 48.6 O, 51.4Al, indicating that the black oxides of the internal oxidation zone are Al_2O_3. The formation of the internal Al_2O_3 oxides is attributed to the fact that a small amount of Al element (0.46 wt.%) is not able to diffuse to the surface of the alloy and is selectively oxidized by oxygen diffused into the interior of the alloy. Kim et al. (Ref 29) have found that the internal Al_2O_3 oxide is formed in the grains and grain boundaries under the oxide scale at the early stage of oxidation. With the progress of oxidation, Al_2O_3 islands become larger and preferentially grow along the grain boundary, resulting in the intergranular

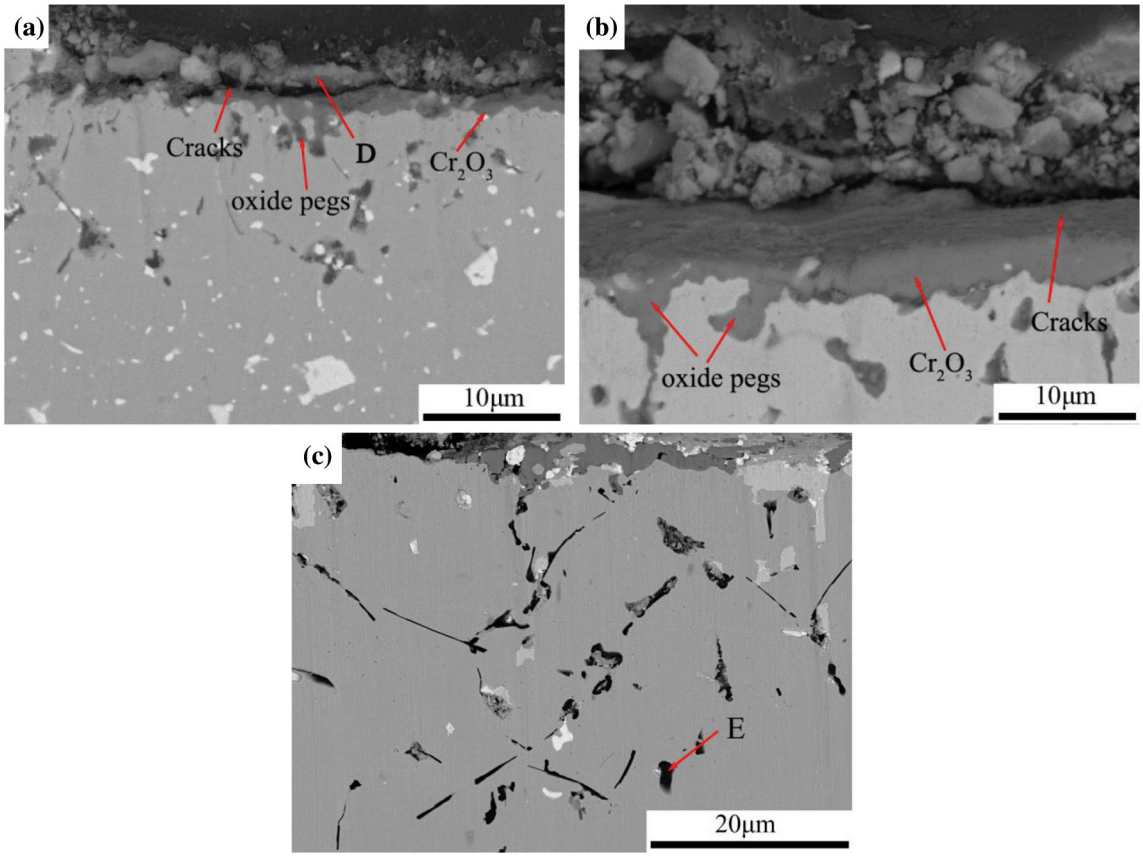

Fig. 4 The cross-sectional morphologies after 100 h oxidation (a) at 900 °C, (b) at 1000 °C and (c) internal oxidation zone at 1000 °C

oxidation. Grain boundaries are fast diffusion channels for oxygen and can be easily oxidized due to the irregular arrangement of atoms and high interface energy. In particular, Ni-based alloys containing a small amount of Al or Cr elements are more prone to internal oxidation and intergranular oxidation (Ref 30). After oxidation at 900 and 1000 °C for 100 h, some oxide pegs are formed at the oxide scales/substrate interface, which can improve the adhesion strength of the oxide scales (Ref 6, 31). In addition, the obvious cracks are observed at the interface between the outer layer and the inner layer, which are mainly related to the growth stress and thermal stress (Ref 3).

In previously published studies, the oxidation behavior of some Ni-based superalloys has also been studied. Cao et al. (Ref 13) have found that GH202 alloy exhibits good oxidation resistance after oxidation at 800 and 900 °C due to the formation of a dense Cr_2O_3 oxidation layer. However, after oxidation at 1000 and 1100 °C, the outer layer shows obvious spalling, which is mainly related to the formation of large and loose $NiCr_2O_4$ and TiO_2. Zheng et al. (Ref 23) have reported that although spinel phases have a certain protective effect due to its low diffusion coefficient to ions or atoms, the formation of $NiCr_2O_4$ generates greater stress in the oxide scale and leads to more serious oxidation effect. In a word, a dense Cr_2O_3 layer as diffusion barrier can prevent the further oxidation of alloys, while the formation and growth of $NiCr_2O_4$ are detrimental to the oxidation resistance of alloys.

The oxidation kinetics and oxides morphologies indicate that the oxidation degree at 1000 °C is much severer than that at 900 °C. The increasing of oxidation temperature promotes the diffusion of alloy elements and oxygen, thus leading to a higher mass gain. Besides, the spinel $NiCr_2O_4$ is the main phase in the oxide scales after oxidation at 1000 °C for 100 h. The formation of $NiCr_2O_4$ consumes protective Cr_2O_3, which accelerates the further oxidation of the superalloy (Ref 26). In addition, the solid-state oxide Cr_2O_3 is oxidized into the volatile CrO_3 at 1000 °C or beyond 1000 °C because of the high oxygen pressure (Ref 21, 32). The formation of gaseous CrO_3 damages the continuity of Cr_2O_3 oxide scale, and results in a severe oxidation effect.

In order to further determine the evolution process and element distribution of the oxide scales, the elemental distribution mappings of Ni-20Cr-18W alloy are shown in Fig. 5 after oxidation at 1000 °C for different time. Figure 5(a) shows the cross-sectional morphology and element distribution of Ni-20Cr-18W alloy oxidized at 1000 °C for 20 h. A dense and continuous single-layer oxide scale is formed on the surface of the alloy, and there is obvious internal oxidation zone under the oxide scale. It can be seen that the dense single-layer oxide scale mainly overlaps with Cr and O elements, so it can be considered that the oxide scale is mainly composed of Cr_2O_3. In addition, the black oxides in the internal oxidation zone are mainly the oxides of Al and O elements, which is consistent with the EDS results in Fig. 4(c). Moreover, it can be seen from the distribution of Cr element that an obvious Cr-depleted region is formed under the Cr_2O_3 layer, with a thickness of about 11 μm. The cross-sectional morphology and element distribution of Ni-20Cr-18W alloy oxidized at 1000 °C for 100 h are shown in Fig. 5(b). The loose outer layer is mainly the oxides of Ni, Cr and O elements, while the dense inner layer is mainly the oxides of Cr and O elements, which corresponds

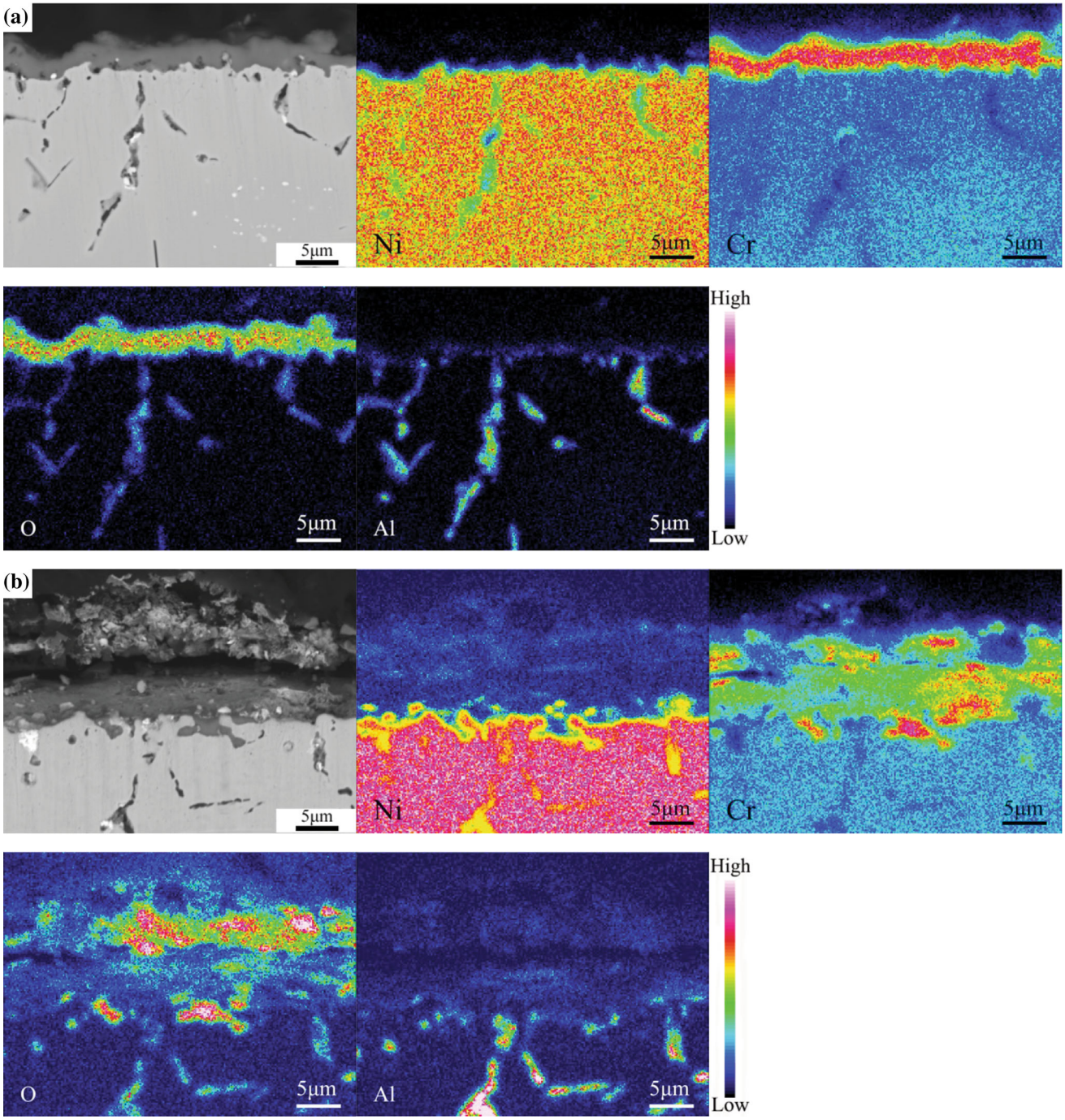

Fig. 5 The elemental transfer of Ni-20Cr-18W alloy after isothermal oxidation at 1000 °C for (a) 20 h and (b) 100 h

to the above analysis. Besides, the black oxides Al_2O_3 are also clearly observed in the internal oxidation zone at 1000 °C for 100 h. Based on the results of the EPMA, it can be concluded that the formation of the oxide scales is a process of evolution from single-layer to double-layer structure at 1000 °C.

3.4 Degradation of Oxide Scales

As shown in Fig. 4, obvious cracking occurs in the oxide scales after oxidation at 900 and 1000 °C for 100 h. The integrity of the oxide scales is very vital to prevent further oxidation of the superalloy. The cracking and spalling of oxide scales are mainly related to the internal stress (Ref 3, 23). The growth stress and thermal stress are the two main internal stresses in the oxide scales. Growth stress is generated during oxidation, and thermal stress is generated in the cooling to room temperature stage (Ref 33-35). Pilling–Bedworth ratio (PBR) is usually used to determine the growth stress and the integrity of oxide scales (Ref 23, 33-35). When PBR $<$ 1, the tensile stress develops in the oxide scales, and the oxide scales cannot cover the alloy surface. When 1 $<$ PBR $<$ 2, dense and protective oxide scales can be formed on the surface of alloys. When PBR $\gg$ 1, the excessive compressive stress in the oxide scales leads to the cracking and spalling of the oxide scales. According to the above analysis results, the outer layer

mainly consists of mixed oxides of Cr_2O_3 and $NiCr_2O_4$, and the inner layer is composed of dense Cr_2O_3 at 900 °C. The PBR of Cr_2O_3 and $NiCr_2O_4$ are 1.29 and 2.05, respectively (Ref 33, 36). Therefore, small compressive stress develops in the inner layer and large compressive stress develops in the outer layer at 900 °C. However, the outer layer consists of a large amount of $NiCr_2O_4$, and the inner layer is composed of dense Cr_2O_3 at 1000 °C. Thus, the outer layer at 1000 °C has larger compressive stress than that at 900 °C. In addition, thermal stress is produced in the cooling stage due to the different coefficient of thermal expansion (CTE) between oxide scales and alloy. The CTE of Cr_2O_3 and $NiCr_2O_4$ is 9.6×10^{-6} K^{-1} (25-1400 °C), 7.6×10^{-6} K^{-1} (25-900 °C), respectively, while the CTE of Ni-Cr-W-based superalloy (Haynes 230 alloy) is about 15.2×10^{-6} K^{-1} (25-800 °C) (Ref 3, 37). Therefore, it can be considered that the thermal stress is also the compressive stress in the outer and inner oxide scales. Also, the increasing of the oxide layer thickness certainly results in the development of larger internal stress in the oxide scales. After oxidation at 900 and 1000 °C, schematic diagram of the internal stress and cracking in the oxide scales is shown in Fig. 6. Based on these analyses, it can be concluded that cracking and spalling of oxides scales are caused by growth stress and thermal stress. The cracking and spalling of the oxide scales are more severe at 1000 °C than that at 900 °C because the outer layer has greater internal stress at 1000 °C. The cracking and spalling of oxide scales mean that the alloy suffers from serious oxidation. The formation of cracks leads to more oxygen to diffuse into the alloy, thus accelerating the further oxidation of the alloy. Weng et al. (Ref 38) have found that the addition of Nb and Y elements can promote the formation of a dense and thin oxide scale, and the rare-earth element Y can also reduce the residual stress in the oxide scale. Tawancy et al. (Ref 39) have revealed that adding a small amount of La, Si and Mn can make the high-temperature thermal stability of Cr_2O_3 be extended to 1150 °C. In general, the cracking and spalling of oxide scales can be improved by reducing the oxidation volatilization of Cr_2O_3 at high temperature, decreasing the internal stress of oxide scales and improving the compactness and adhesion of oxide scales.

3.5 Oxidation Mechanism

The evolution of the oxide scales on Ni-20Cr-18W superalloy at 1000 °C is shown in Fig. 7. Based on the above results and discussion, the oxidation behavior of the Ni-20Cr-18W superalloy can be summarized as follows. At the beginning, oxygen molecules are adsorbed on the alloy surface and decomposed into oxygen atoms, while Cr element diffuses outward from the substrate. Thus, Cr_2O_3 nucleate and grow on the surface of the alloy (Fig. 7a). This reaction stage is controlled by the inward diffusion of oxygen and the outward diffusion of Cr. With the increasing of oxidation time, a large amount of Cr diffuses outward due to its higher affinity to oxygen than Ni (Ref 5). Therefore, a dense and continuous Cr_2O_3 layer is formed on the surface of Ni-20Cr-18W superalloy (Fig. 7b). At the same time, as shown in Fig. 4(c), the internal oxidation zone is also formed under the oxide scales, which is mainly attributed to the fact that a small amount of Al element (0.46 wt.%) is selectively oxidized by oxygen diffused into the interior of the alloy. The outward diffusion of Ni element increases gradually due to the depletion of Cr element in the substrate alloy. Meanwhile, the formed NiO reacts with Cr_2O_3 to form spinel $NiCr_2O_4$ in the oxide scales (Fig. 7c) (Ref 26, 40). As oxidation proceeds, the concentration of Cr decreases below the critical value for the formation of oxides. Therefore, a large amount of Ni begins to diffuse outward through the oxide scales to form oxides. However, NiO and Cr_2O_3 cannot exist stably at high temperature, so a large amount of $NiCr_2O_4$ oxide is formed in the outer layer of the oxide scales (Fig. 7d). Compared with oxidation at 1000 °C, the consumption of Cr and the outward diffusion of

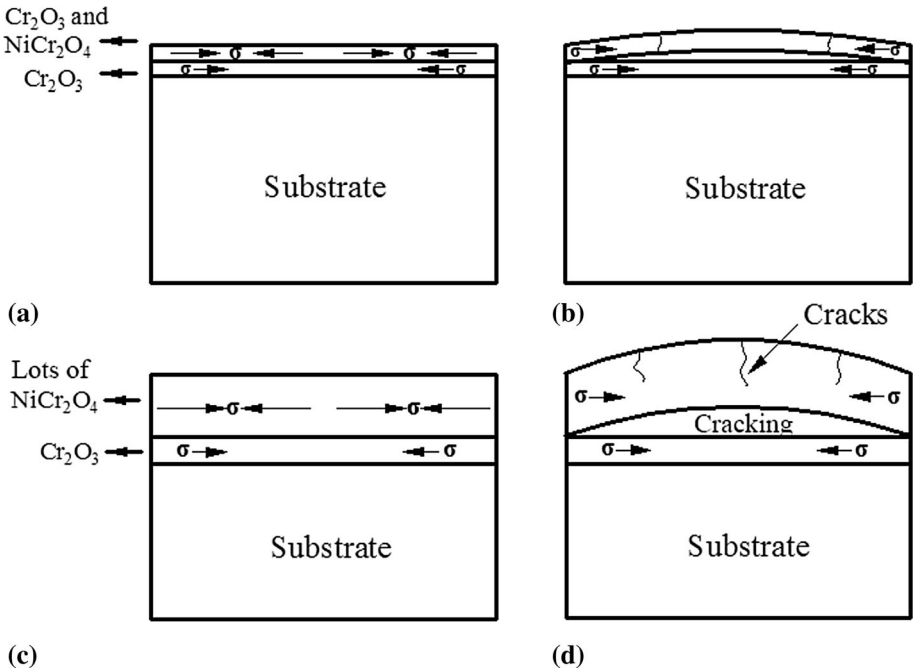

Fig. 6 Schematic diagram of internal stress and cracking in oxide scales (a) internal stress of the oxide scales at 900 °C, (b) cracking of the oxide scales at 900 °C, (c) internal stress of the oxide scales at 1000 °C and (d) cracking of the oxide scales at 1000 °C

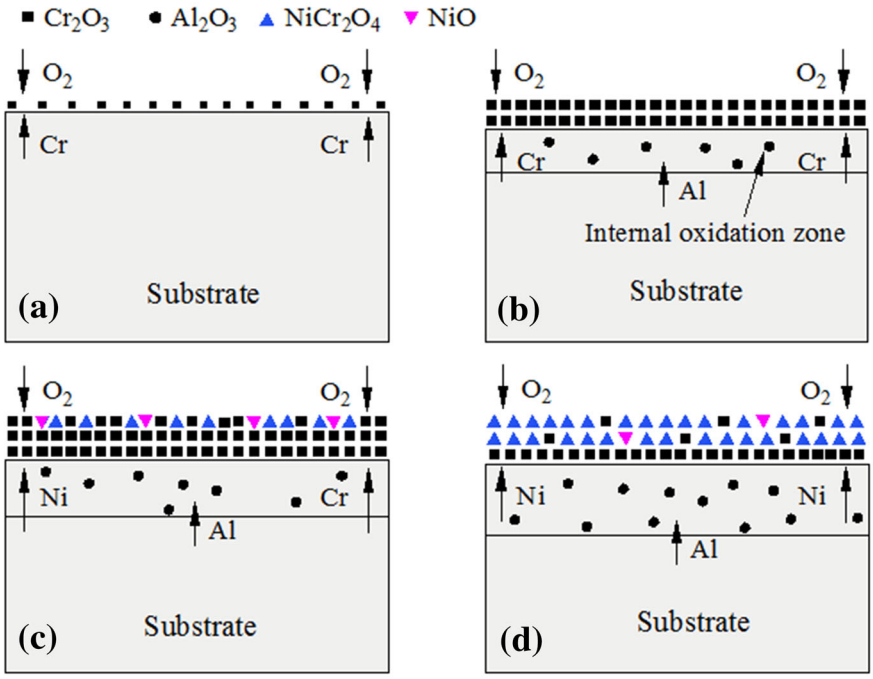

Fig. 7 Oxidation mechanism of Ni-20Cr-18W superalloy at 1000 °C (a) nucleation and growth of Cr_2O_3, (b) formation of Cr_2O_3 layer and internal oxidation zone, (c) outward diffusion of Ni and (d) formation of oxide scales

Ni are both slowed down at 900 °C, causing a light oxidation attack at 900 °C.

4. Conclusion

(1) The mass gain of the Ni-20Cr-18W superalloy increases with time and temperature, and the oxidation kinetics follows a parabolic oxidation law at both 900 and 1000 °C. The oxidation rate constant K is 4.066×10^{-13} and 2.863×10^{-12} g^2 cm^{-4} s^{-1} at 900 and 1000 °C, respectively.

(2) The outer layer of the oxide scales is mainly composed of mixed oxides of Cr_2O_3 and $NiCr_2O_4$, and the inner layer is Cr_2O_3 at 900 °C. During oxidizing at 1000 °C, the oxide scales evolve from dense Cr_2O_3 single-layer structure to double-layer structure which consists of inner Cr_2O_3 layer and outer layer composed of lots of $NiCr_2O_4$, Cr_2O_3 and a small amount of NiO, and the size and content of $NiCr_2O_4$ are relatively larger than that of 900 °C. The internal oxidation zone dispersed with Al_2O_3 is formed under the oxide scales at both 900 and 1000 °C.

(3) The obvious cracks are observed at the interface between the outer layer and the inner layer after oxidation at 900 and 1000 °C for 100 h, which is mainly related to the growth stress during oxidation and thermal stress in the cooling stage.

References

1. R.C. Reed, *The Superalloys Fundamentals and Applications*, Cambridge University, Cambridge, 2006
2. F.H. Latief, K. Kakehi, and Y. Tashiro, Oxidation Behavior Characteristics of An Aluminized Ni-Based Single Crystal Superalloy CM186LC Between 900 °C and 1100 °C in Air, *J. Ind. Eng. Chem.*, 2013, **19**(6), p 1926–1932
3. L. Zheng, M. Zhang, R. Chellali, and J. Dong, Investigations on the Growing, Cracking and Spalling of Oxides Scales of Powder Metallurgy Rene95 Nickel-Based Superalloy, *Appl. Surf. Sci.*, 2011, **257**(23), p 9762–9767
4. M. Bensch, J. Preußner, R. Hüttner, G. Obigodi, S. Virtanen, J. Gabel, and U. Glatzel, Modelling and Analysis of the Oxidation Influence on Creep Behaviour of thin-walled structures of the single-crystal nickel-base superalloy René N5 at 980 °C, *Acta Mater.*, 2010, **58**(5), p 1607–1617
5. L. Zheng, M. Zhang, and J. Dong, Oxidation Behavior and Mechanism of Powder Metallurgy Rene95 Nickel Based Superalloy Between 800 and 1000 °C, *Appl. Surf. Sci.*, 2010, **256**(24), p 7510–7515
6. D.W. Yun, S.M. Seo, H.W. Jeong, and Y.S. Yoo, The Effects of the Minor Alloying Elements Al, Si and Mn on the Cyclic Oxidation of Ni-Cr-W-Mo Alloys, *Corros. Sci.*, 2014, **83**, p 176–188
7. A. Keyvani, M. Saremi, and M.H. Sohi, Oxidation Resistance of YSZ-Alumina Composites Compared to Normal YSZ TBC Coatings at 1100 °C, *J. Alloys Compd.*, 2011, **509**(33), p 8370–8377
8. K. Zhang, T. Zhang, and L. Song, Oxidation Behavior of a High-Nb-Containing TiAl Alloy with Multilayered Thermal Barrier Coatings, *J. Therm. Spray Technol.*, 2018, **27**, p 999–1010
9. S. Saladi, J. Menghani, and S. Prakash, A Study on the Cyclic Oxidation Behavior of Detonation-Gun-Sprayed Ni-5Al Coatings on Inconel-718 at 900 C, *J. Mater. Eng. Perform.*, 2014, **23**(12), p 4394–4403
10. A. Pfennig and B. Fedelich, Oxidation of Single Crystal PWA 1483 at 950 °C in Flowing Air, *Corros. Sci.*, 2008, **50**(9), p 2484–2492
11. H. Asteman, W. Hartnagel, and D. Jakobi, The Influence of Al Content on the High Temperature Oxidation Properties of State-of-the-Art Cast Ni-base Alloys, *Oxidation of Metals*, 2013, **80**(1-2), p 3–12
12. H.T. Mallikarjuna, W.F. Caley, and N.L. Richards, Oxidation Kinetics and Oxide Scale Characterization of Nickel-Based Superalloy IN738LC at 900 °C, *J. Mater. Eng. Perform.*, 2017, **26**(10), p 4838–4846
13. J. Cao, J. Zhang, R. Chen, Y. Ye, and Y. Hua, High Temperature Oxidation Behavior of Ni-Based Superalloy GH202, *Mater. Charact.*, 2016, **118**, p 122–128

14. S.J. Park, S.M. Seo, Y.S. Yoo, H.W. Jeong, and H.J. Jang, Effects of Al and Ta on the High Temperature Oxidation of Ni-Based Superalloys, *Corros. Sci.*, 2015, **90**(5), p 305–312
15. L. Klein, Y. Shen, M.S. Killian, and S. Virtanen, Effect of B and Cr on the High Temperature Oxidation Behaviour of Novel γ/γ′-Strengthened Co-base Superalloys, *Corros. Sci.*, 2011, **53**(9), p 2713–2720
16. X.J. Peng, K.Y. Chen, R. Liu, and M. Liang, Modeling Study of Cyclic Oxidation Behavior of NiAl and NiCr Alloys, *J. Mater. Eng. Perform.*, 2014, **23**(12), p 4366–4373
17. J. Wang, L. Yuan, R. Hu, T. Zhang, and J. Li, Effect of Lanthanum on Oxidation Behavior of Ni-20Cr-18W-1Mo Alloys at 1373 K for 100 h in Air, *Rare Metal Mate. Eng.*, 2014, **43**(9), p 2060–2063
18. D.W. Yun, S.M. Seo, H.W. Jeong, and Y.S. Yoo, The Cyclic Oxidation Behaviour of Ni-Based Superalloy GTD-111 with Sulphur Impurities at 1100 °C, *Corros. Sci.*, 2015, **90**, p 392–401
19. M. Wu, M. Chen, S. Zhu, and F. Wang, Effect of Sand Blasting on Oxidation Behavior of K38G Superalloy at 1000 °C, *Corros. Sci.*, 2015, **92**, p 256–262
20. S. Hamidi, M.R. Rahimipour, M.J. Eshraghi, S.M.M. Hadavi, and H. Esfahani, Kinetics and Microstructural Investigation of High-Temperature Oxidation of IN-738LC Super Alloy, *J. Mater. Eng. Perform.*, 2016, **26**(2), p 563–570
21. C.T. Liu, J. Ma, and X.F. Sun, Oxidation Behavior of a Single-Crystal Ni-Base Superalloy Between 900 and 1000 °C in Air, *J. Allos Compd.*, 2010, **491**(1-2), p 522–526
22. T.-B. Zhang, R.-F. Dong, R. Hu, H.-C. Kou, and J.-S. Li, Hot Corrosion Characteristics of Ni-20Cr-18W Superalloy in Molten Salt, *Trans. Nonferrous Met. Soc. China*, 2015, **25**(11), p 3840–3846
23. L. Zheng, M.C. Zhang, R. Chellali, H. Bouchikhaoui, and J.X. Dong, Oxidation Property of Powder Metallurgy EP741NP Ni Based Superalloy at Elevated Temperatures, *Mater. Technol.*, 2013, **28**(3), p 122–128
24. D. Saber, I.S. Emam, and R. Abdel-Karim, High Temperature Cyclic Oxidation of Ni Based Superalloys at Different Temperatures in Air, *J. Alloys Compd.*, 2017, **719**, p 133–141
25. A. Duval, F. Miserque, M. Tabarant, J.P. Nogier, and A. Gédéon, Influence of the Oxygen Partial Pressure on the Oxidation of Inconel 617 Alloy at High Temperature, *Oxid. Met.*, 2010, **74**(5-6), p 215–238
26. C.T. Liu, X.F. Sun, H.R. Guan, and Z.Q. Hu, Oxidation of the single-crystal Ni-base superalloy DD32 containing rhenium in air at 900 and 1000 °C, *Surf. Coat. Technol.*, 2005, **197**(1), p 39–44
27. T. Zengwu, H. Rui, and L. Jinshan, Isothermal Oxidation Behavior of Ni-20Cr-18W Superalloy at 1100 °C, *Rare Met. Mater. Eng.*, 2012, **41**(12), p 2081–2085
28. X. Gong, R.R. Chen, Y.H. Yang, Y. Wang, H.S. Ding, J.J. Guo, Y.Q. Su, and H.Z. Fu, Effect of Mo on Microstructure and Oxidation of NiCoCrAlY Coatings on High Nb Containing TiAl Alloys, *Appl. Surf. Sci.*, 2018, **431**, p 81–92
29. D. Kim, C. Jang, and W.S. Ryu, Oxidation Characteristics and Oxide Layer Evolution of Alloy 617 and Haynes 230 at 900 °C and 1100 °C, *Oxid. Met.*, 2009, **71**(5–6), p 271–293
30. G.C. Wood, F.H. Stott, D.P. Whittle, Y. Shida, and B.D. Bastow, The high-temperature internal oxidation and intergranular oxidation of nickel-chromium alloys, *Corros. Sci.*, 1983, **23**(1), p 25
31. H. Buscail, S.E. Messki, F. Riffard, S. Perrier, R. Cueff, E. Caudron, and C. Issartel, Characterization of the Oxides Formed at 1000 °C on the AISI, 316L Stainless Steel—Role of Molybdenum, *Mater. Chem. Phys.*, 2008, **111**(2-3), p 491–496
32. H. Xiaoxiao, L. Jinshan, H. Rui, B. Guanghai, and F. Hengzhi, Evolution of Oxidation in Ni-Cr-W Alloy at 1100 °C, *Rare Met. Mater. Eng.*, 2010, **39**(11), p 1908–1911
33. C. Xu and W. Gao, Pilling-Bedworth Ratio for Oxidation of Alloys, *Mater. Res. Innov.*, 2000, **3**(4), p 231–235
34. S.R.J. Saunders, M. Monteiro, and F. Rizzo, The Oxidation Behaviour of Metals and Alloys at High Temperatures in Atmospheres Containing Water Vapour: A Review, *Prog. Mater Sci.*, 2008, **53**(5), p 775–837
35. H.E. Evans and R.C. Lobb, Conditions for the Initiation of Oxide-Scale Cracking and Spallation, *Corros. Sci.*, 1984, **24**(3), p 209–222
36. E.P. Busso, H.E. Evans, Z.Q. Qian, and M.P. Taylor, Effects of Breakaway Oxidation on Local Stresses in Thermal Barrier Coatings, *Acta Mater.*, 2010, **58**(4), p 1242–1251
37. L. Jian, P. Jian, H. Bing, and G. Xie, Oxidation Kinetics of Haynes 230 Alloy in Air at Temperatures Between 650 and 850 °C, *J. Power Sources*, 2006, **159**(1), p 641–645
38. F. Weng, H. Yu, C. Chen, and K. Wan, High-Temperature Oxidation Behavior of Ni-Based Superalloys with Nb and Y and the Interface Characteristics of Oxidation Scales, *Surf. Interface Anal.*, 2015, **47**(3), p 362–370
39. H.M. Tawancy, Enhancing the Oxidation Performance of Wrought Ni-Base Superalloy by Minor Additions of Active Elements, *J. Mater. Eng. Perform.*, 2016, **25**(12), p 5231–5237
40. F. Weng, H. Yu, C. Chen, and K. Wan, Fabrication of Ni-Based Superalloys Containing Nb and Their High Temperature Oxidation Behaviors, *Mater. Manuf. Process.*, 2015, **30**(11), p 1364–1369

Publisher's Note Springer Nature remains neutral with regard to jurisdictional claims in published maps and institutional affiliations.